AUTOMATED DETECTION OF MECHANICALLY INDUCED BRUISE AREAS IN GOLDEN DELICIOUS APPLES USING FLUORESCENCE IMAGERY

Y. C. Chiu, X. L. Chou, T. E. Grift, M. T. Chen

ABSTRACT. *This study pursues the detection of bruised areas caused by mechanical impact on Golden Delicious apples using chlorophyll fluorescence imagery. When a fruit is impacted by a mechanical force and a bruise occurs, the chlorophyll nuclei inside the peel are damaged, which causes a reduction in fluorescence excitation compared to non-impacted areas. This difference allows automated detection of bruises and removal of damaged fruits to maintain optimal quality. In this study, fruit bruises were created using impact forces of 68.6, 88.2, and 107.8 N, and the resulting damage to chlorophyll nuclei inside the fruit peel was observed. Expansion of the area of damaged chlorophyll nuclei over time was observed using fluorescence imagery 0.5, 1, 2, and 4 h after the mechanical impact. This study employed a continuous capture of fruit fluorescence images and used MATLAB software for image processing and analysis. Edge contour noise was filtered by presetting a proper threshold, and the contour features of fruit bruises were distinguished using local adaptive binarization and a size filter. The experimental results showed that the mean recognition rate of a bruise 0.5 h after impact forces of 68.6, 88.2, and 107.8 N was as high as 86.7%, and the bruise recognition rate 1 h after impact was 100%. In conclusion, the fluoroscopic examination system for bruises was capable of detecting bruises accurately before the bruises were visible to the naked eye.*

Keywords. *Adaptive binarization, Chlorophyll, Image processing, Non-destructive inspection.*

Fruit tissues, which contain large amounts of chlorophyll, are susceptible to damage from mechanical impact. This damage has an effect on photosynthetic activity, which in turn reduces the fluorescence of the cells. The reduced fluorescence can be detected using machine vision, which allows for removal of the damaged fruits in an automated fashion. Jacobi (1998) studied the relationship between peel surface color and chlorophyll fluorescence in Jin-Hwang mangos during the maturing stage. Song et al. (1997) observed variability in the chlorophyll fluorescence of apples after controlled-atmosphere storage and cold storage, which allowed post-storage quality assessment. Nedbal et al. (2000) observed the chlorophyll fluorescence of lemons and established a disease index that enabled prediction of biological and non-biological damage. Bron et al. (2004) conducted multiple regression forecasting of the shelf life of fruit based on fluorescence parameters, firmness, and skin hues.

Many studies have focused on bruise detection in apples. El Masry et al. (2008) developed a hyperspectral imaging system based on the spectral region between 400 and 1000 nm to detect bruises on McIntosh apples. Moshou et al. (2005) found that fluorescence imagery has the potential to assess mealiness, and senescence in general. This method could be used to predict the period in which a certain quality level can be guaranteed to consumers. Xing et al. (2005) developed a hyperspectral imaging system using the spectral region between 400 and 1000 nm to detect bruises on 'Golden Delicious' apples. An image processing and classification algorithm based on moments thresholding was developed. The results indicated that approximately 93% of non-bruised apples were recognized as sound, and an accuracy of approximately 86% was achieved in the detection of bruises. Ariana et al. (2006) used multispectral imaging in reflectance and fluorescence mode to detect various defects on three varieties of apple. Artificial neural network (ANN) classification models were developed, and the technique showed promise for accurate recognition of various types of defects.

Closely related to this research, Rehkugler and Throop (1986) developed an apple handling and sorting device using machine vision for bruise detection and classification, which determined the bruise patterns by image filtering, differencing, and binary image thresholding, and measured the shape of the areas representative of bruises by using thinness ratios. Martinsen et al. (2014) quantified the diffuse reflectance change caused by fresh bruises on apples, which can aid in the design of instruments and algorithms for rapid identification of fresh bruises in apples to amelio-

Submitted for review in January 2014 as manuscript number ITSC 10578; approved for publication by the Information, Technology, Sensors, & Control Systems Community of ASABE in January 2015.

The authors are **Yi-Chich Chiu, ASABE Member,** Professor, and **Xing-Liang Chou,** Research Assistant, Department of Biomechatronic Engineering, National Ilan University, Taiwan; **Tony E. Grift, ASABE Member,** Associate Professor, Department of Agricultural and Biological Engineering, University of Illinois, Urbana, Ill.; **Mu-Te Chen,** Former Graduate Student, Department of Biomechatronic Engineering, National Ilan University, Taiwan. **Corresponding author:** Yi-Chich Chiu, National Ilan University, No. 1, Section 1, Shen-Lung Road, Yilan 26041, Taiwan; phone: +886-3-9357400, ext. 7804; e-mail: yichiu@niu.edu.tw.

Vol. 58(2): 215-225 ISSN 2151-0032 DOI 10.13031/trans.58.10578

rate handling and grading problems. Xing and Baerdemaeker (2007) used a spectrophotometric method for detecting fresh bruises on apples by predicting the softening index, which is related to the elasticity modulus of the tissue. Diffuse reflectance spectra were acquired with a spectrophotometer in the wavelength region between 400 and 1700 nm. Ma et al. (2014) detected bruises and pest infestation simultaneously on Golden Delicious apples, helping to classify the quality and safety of apples during postharvest sorting and grading.

The objectives of this study were to (1) develop a method allowing precise impacts on apples to produce fresh bruises and (2) use chlorophyll fluorescence images for automatic detection of bruise areas on Golden Delicious apples to accurately detect fresh bruises 0.5 h after impact, before the bruises are visible to the naked eye. Hopefully, the developed methodologies will aid in the design of an on-line apple bruise detection system for real-world application in the future.

Materials and Methods

This study used the Golden Delicious apple as the object. Prior to the tests, the test apples were taken from the refrigerator and kept at 25°C for two days in order to restore the apples to their original condition before packing.

Experimental Equipment

Two main experimental instruments were used in this study: a fruit impact device and a fruit bruise fluorescence detection system. The fruit impact device produces the apple bruises, and the fruit bruise fluorescence detection system detects and analyzes the bruises on the apples.

Fruit Impact Device

This study used a fruit impact device based on the pendulum principle (Chen, 2009) to accurately control the impact force that creates apple bruises (fig. 1). This impact force was measured using a dynamic force gauge (208C02, PCB Piezotronics, Inc., Depew, N.Y.), a signal conditioner (480C02, PCB Piezotronics, Inc.), and a digital oscilloscope with an embedded signal acquisition card (TDS1012B, Tektronix, Inc., Beaverton, Ore.). LabVIEW SignalExpress 2.0 (National Instruments, Austin, Tex.) was used to develop the impact force capture analysis system. In the force

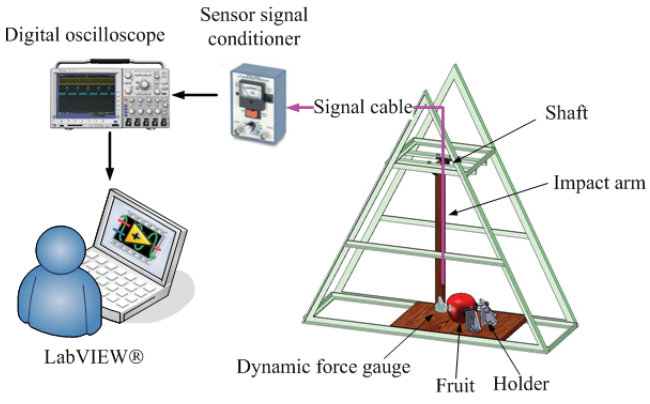

Figure 1. System structure of fruit impact device (Chen, 2009).

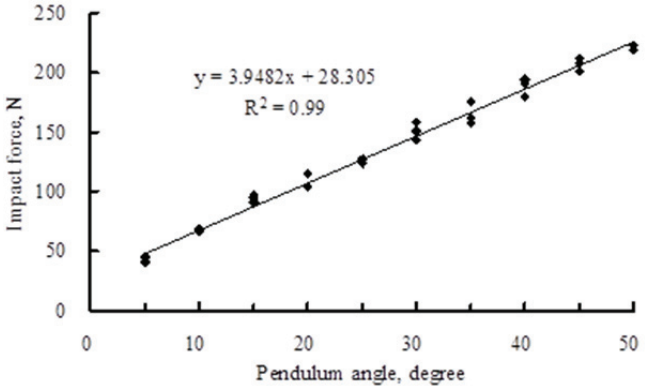

Figure 2. Relationship between pendulum angle and peak value of impact force.

measuring process, only a first-time impact on the apple was allowed, and the impact force was recorded by the system. To avoid further impacts on the apple, the impact arm was seized by the operator after the first impact, and the force curve displayed on the computer screen was examined to ensure that the impact experiment was successful. To assess the operation of the fruit impact device, the relationship between the angle (in degrees) and the impact force (in N) was determined. Figure 2 shows the relationship between the initial drop angle of the pendulum and the first-time impact force of the fruit impact device (R^2 = 0.99).

Fruit Bruise Fluorescence Detection System

The fruit bruise fluorescence detection system (Chen, 2009) used a 470 nm wavelength LED as the fluorescence excitation source. To capture the emissive fluorescence, a digital camera (CV-A50IR, JAI A/S, Glostrup, Denmark) with a 650 nm high-pass filter lens was employed (fig. 3). The camera was controlled with an analog image acquisition card (PCI-1411, National Instruments), and the excitation source was controlled with a digital I/O device (USB-6008, National Instruments). LabVIEW version 8.5 was used for the development of the bruise detection system, which allowed setting the image capture frequency as well as the gain for the CCD image signal.

Fluorescence Image Processing and Analysis

The fluorescence intensity varies with time, and there is an increasing difference between the fluorescence intensity of a bruised area compared to the undisturbed peel. To measure the fluorescence intensity over time, a MATLAB program was developed that captured images every second. To ensure correct measurements, one fruit fluorescence image per second was captured after the apple was impacted, and the bruise features were determined by accumulating various numbers of images from 5 to 60 s. The optimal accumulated image calculation method was determined by comparing the accuracy rates of bruise area detection.

Figure 4 shows a flowchart of the fruit bruise detection process. As shown in figure 4, the system captures the first apple fluorescence image and calculates the bruise feature of the fluorescence image. The analyzed image is stored in the bruise feature database after image processing. The

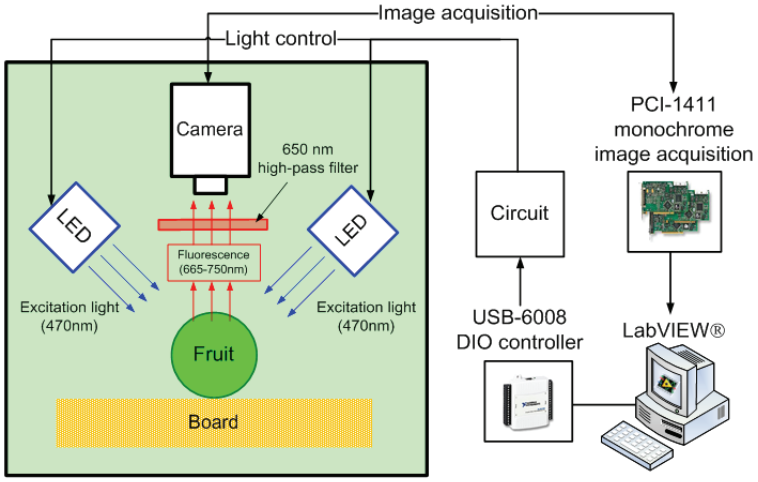

Figure 3. Schematic diagram of fruit bruise fluorescence detection system (Chen, 2009).

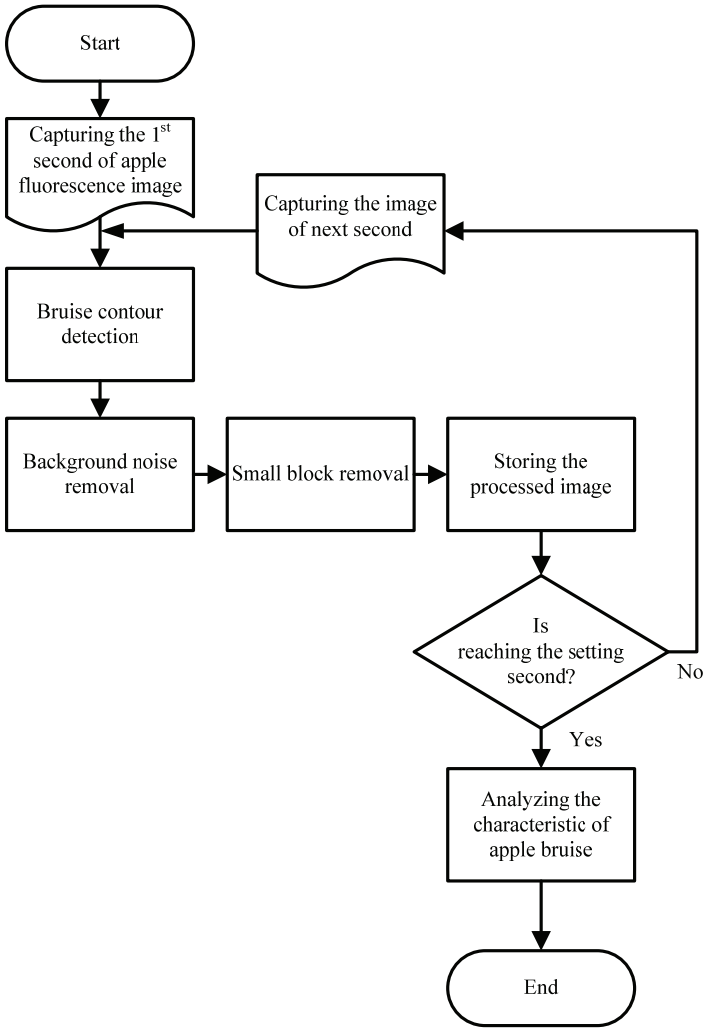

Figure 4. Flowchart of the fruit bruise detection process.

system then captures and analyzes the bruise feature of the next apple fluorescence image with an interval of 1 s until the number of captured fluorescence images in the database reaches the preset threshold.

Since the fluorescence intensity of the bruised area after impact is weaker than that of adjacent pixels, the bruise contour can be determined using a local adaptive binarization method. The edge of the bruise is not continuous but instead contains noisy edges caused by varying illumination angles. To alleviate this problem, a size filter was ap-

plied that yields quasi-continuous edges. A size filter was also used to remove the small noise blocks on the fruit surface, such as spots and concavity. The image processing and analysis methods are described in the following sections.

BRUISE CONTOUR DETECTION

The contour features of fruit bruises were distinguished using a local adaptive binarization method. The first step in the detection of bruises is thresholding. The fluorescence images enhance the appearance of both the bruise and other defective spots on the surface of the apple. These morphological features prohibit global image thresholding, in which a single parameter separates the bruise-related pixels from the remainder of the apple. To alleviate this problem, local image thresholding was applied in which the fluorescence image was divided into a series of smaller subimages that were thresholded separately. The following steps were used in this process:

1. The original fluorescence image was plotted with a masking window of $M \times M$ pixels (indicated by the M-value in this article), and the mean of the pixels in this area was determined as threshold value $H_{1,1}$, as shown in figure 5a.
2. After shifting to the right across $M/2$ pixels, step 1 was repeated to determine the second threshold value ($H_{1,2}$ in fig. 5b). In general, scanning $M/2$ pixels horizontally (x) and vertically (y) was done to calculate the corresponding $H_{x,y}$ values. Therefore, the original fruit fluorescence image's $N \times N$ pixels contained $(2N/M)-1 \times (2N/M)-1$ $H_{x,y}$ threshold values.
3. As shown in figure 5c, bilinear interpolation was used for four adjacent H-values ($H_{x,y}$, $H_{x+1,y}$, $H_{x,y+1}$, and $H_{x+1,y+1}$) to determine the adaptive threshold value $R_s(i,j)$ corresponding to the $M/2 \times M/2$ area.
4. By comparing each pixel $P(i,j)$ of the original fruit fluorescence image (fig. 6a) with the calculated adaptive threshold value $R_s(i,j)$ by using equation 1 (fig. 6b), the pixels $P_{Label}(i,j)$ of the depressed bruise area on the fruit were detected, and the result is shown in figure 6c:

$$P_{Label}(i,j) = \begin{cases} 1 \text{ if } P(i,j) \le R_S(i,j) \\ 0 \text{ otherwise} \end{cases} \quad (1)$$

BACKGROUND NOISE REMOVAL

In the fruit bruise fluorescence detection system, the light source is directed toward the center of the apple, so the fluorescence excited around the contour is vague. To determine the proper threshold value for binarization, the Ostu method (method of maximum between-cluster variance, or MBV) was employed (Ostu, 1979). This method removed noise outside the apple contour from the local adaptive binarization image produced earlier and obtained the apple bruise feature from the result of local adaptive binarization processing of $P_{Label}(i,j)$. The calculation procedure is as follows:

1. Select an initial estimated threshold value T_i (the suggested value is the median between the maximum and minimum gray-scale values of the image).

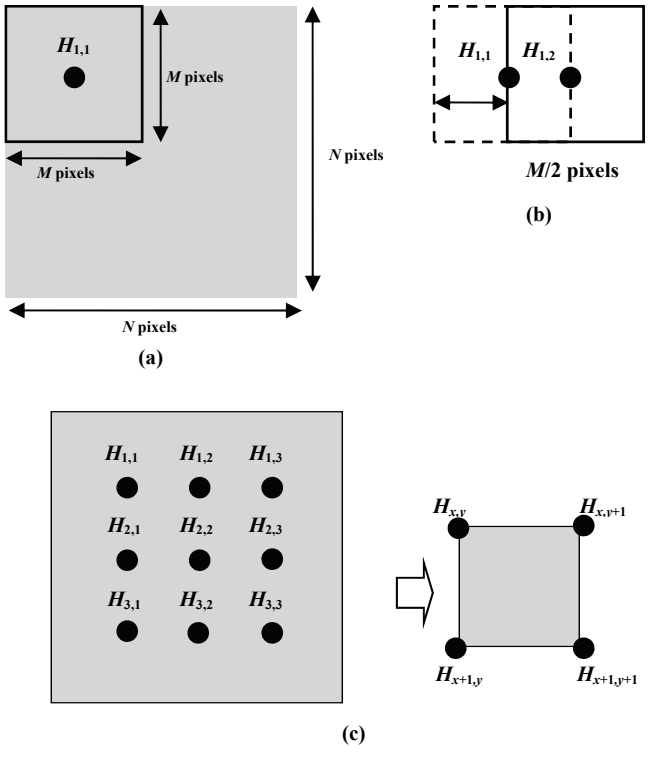

Figure 5. Schematic of local adaptive binarization process: (a) calculate the adaptive threshold value $H_{1,1}$ representing the local $M \times M$ block, (b) calculate another $H_{1,2}$ value after $M/2$ shift, and (c) determine the bilinear interpolation value for the four adjacent $H_{i,j}$ values to the threshold value corresponding to each pixel.

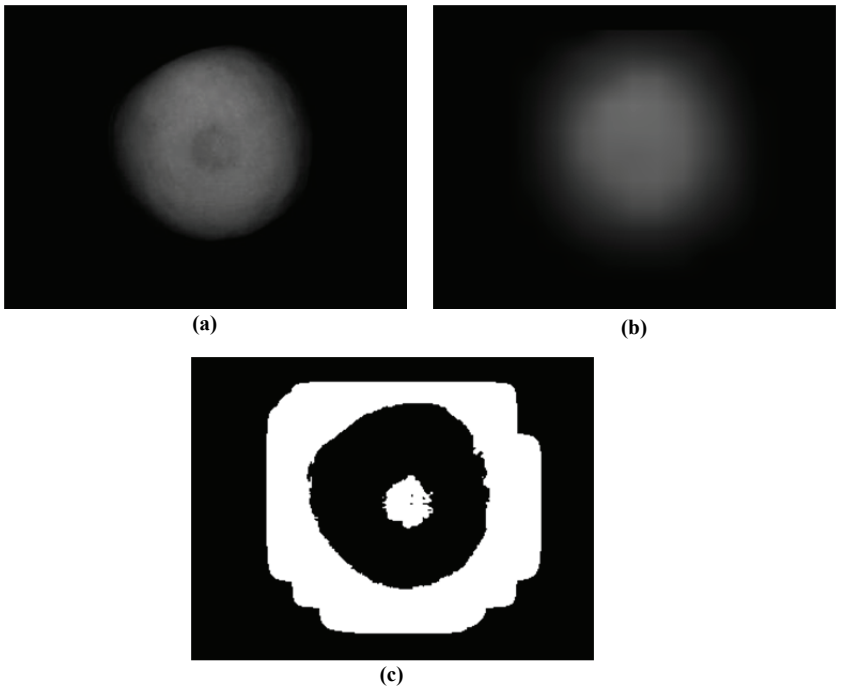

Figure 6. Identification of bruise area on apple by using local adaptive binarization: (a) original fluorescence image $P(i,j)$, (b) adaptive threshold value $R_s(i,j)$, and (c) result of local adaptive binarization processing $P_{Label}(i,j)$.

2. Using the T_i value as the threshold, divide the image into two groups of pixels: G_1 represents all pixels with gray-scale values $\geq T_i$, and G_2 represents all pixels with gray-scale values $< T_i$.
3. Calculate the mean gray-scale values μ_1 and μ_2 of the pixels in G_1 and G_2, respectively.
4. Determine the new threshold value using equation 2:

$$T_{new} = \frac{\mu_1 + \mu_2}{2} \tag{2}$$

5. Determine if the absolute difference of T_i and T_{new} is less than the tolerance coefficient (k_0). If so, then the final T_{new} is designated as the overall threshold value (T_{all}); otherwise, T_i is replaced by T_{new}, and steps 2 through 4 are repeated. This study set k_0 at 0.5. If the absolute difference of T_i and T_{new} is less than 0.5, then T_i and T_{new} are converged at the same integral gray level, and the gray level is counted by integral point.
6. Determine the apple bruise feature $P_{bruise}(i,j)$ using equation 3:

$$P_{bruise}(i,j) = \begin{cases} 1 \text{ if } P_{Label}(i,j) \geq T_{all} \\ 0 \text{ otherwise} \end{cases} \tag{3}$$

Figure 7a shows an apple contour identified with the preceding steps. The coordinates of the contour that are likely to be misjudged are removed from the local adaptive binarization, $P_{Label}(i,j)$, using equation 3. The resulting bruise feature, $P_{bruise}(i,j)$, is shown in figure 7b.

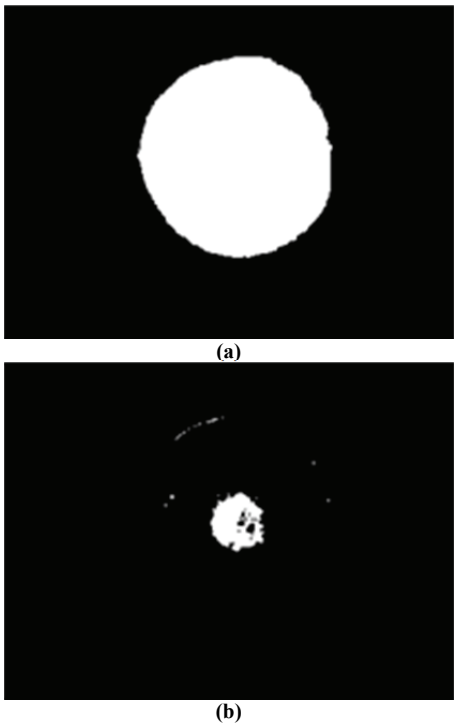

Figure 7. Results of background noise removal for bruised apple: (a) apple contour identification and (b) bruise feature, $P_{bruise}(i,j)$, obtained after background noise removal.

SMALL BLOCK REMOVAL

After background noise removal, the bruise features in the fluorescence images of the last several seconds were overlapped, and a threshold was used to determine the final bruise contour. The bruise area detection process was hampered by two effects: (1) the individual fluorescence images contained noise inside the assumed bruised area, and (2) the

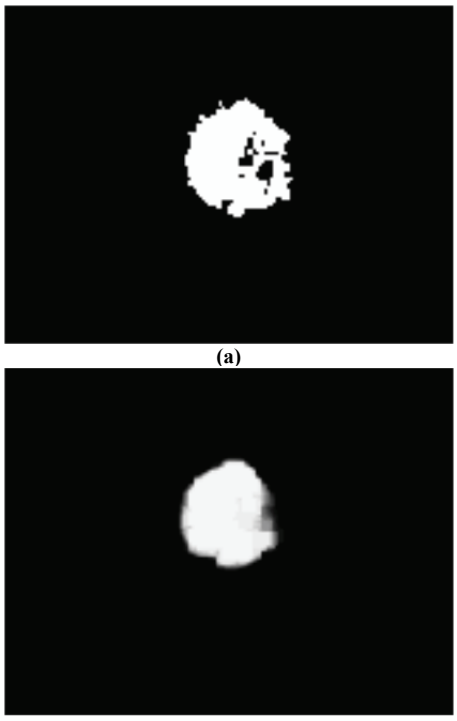

Figure 8. Results of small block removal for bruised apple: (a) binary image after noise removal and (b) bruise feature after several seconds of image overlapping.

fluorescence emitted by the bruised area changed over time. To address the first problem, a size filter was employed that discarded connected noisy pixel blocks smaller than an arbitrary size. After this process, the second problem was addressed by taking the average values of a certain number of fluorescence images that were taken within the same number of seconds. The averaged images were subsequently used to assess whether the assumed bruised area represented a true bruise.

Figure 8a shows a binary image of the fluorescence emission after noise removal, and figure 8b shows the resulting image using the average of a certain number of images that were taken within the same number of seconds. The optimum number of sampled images (i.e., sampling duration) needed was left to be determined by the experiments. Therefore, the bruised area can be automatically calculated by the system through the process of bruise contour detection, background noise removal, and small block removal, as shown in figure 8b. This study manually identified the bruise area in the fluorescence images, compared that area with the bruise area detected by the system, and then calculated the accuracy rate to evaluate the system performance.

EXPERIMENTS

To demonstrate the developed methodology of automated bruise detection, it was necessary to determine if the proposed fruit bruise detection system can successfully detect fruit bruises. To determine the time for the bruised area to be detected after the apples were impacted by the different forces, experiments were conducted to establish appropriate image processing parameters after different mechanical impact forces. The tests consisted of impacting 25 Golden Delicious apples with forces of 68.6, 88.2, and 107.8 N, and bruise detection accuracy was evaluated at 0.5, 1, 2, and 4 h after impact. The impact forces were chosen based on preliminary observations.

RESULTS AND DISCUSSION

Two parameters that influence the success rate of bruise detection are the *M*-value originating from the local adaptive binarization procedure and the number of averaged images needed. The *M*-value should consider the pixels in the bruise area. The number of averaged images can increase the accuracy of bruise detection, as an image of a single time point is likely to vary with the fluorescence excitation and reduce the accuracy of determining the bruise features. However, a larger number of averaged images requires more time for analysis. The experimental results are described in the following sections.

EFFECT OF *M*-VALUE ON DETECTION ACCURACY

The original size of the captured images was 320 × 240 pixels, and apple-related pixels accounted for 28% of the full image. The images were cropped to 200 × 200 pixels to facilitate image processing, after which the apple-related pixels accounted for 53.8% of the image. A total of 30 fluorescence images of the first 30 s were taken for use in detecting bruises.

The primary experimental result showed when the *M*-value was less than 20, a slight change in fluorescence was likely to be regarded as a bruise area, and the computing speed of the system was low. When the *M*-value was greater than 50, the detected bruise area was vague. Therefore, three *M*-values (masking window sizes of 25, 40, and 50 pixels) were used for further analysis. The system-calculated fruit bruise area ($Area_{sys}$) accumulated all the bruise points, $P_{bruise}(i,j)$, according to equation 4:

$$\text{Area}_{sys} = \sum_{i=1,\,j=1}^{i=M,\,j=N} P_{bruise}(i,j) \tag{4}$$

To determine the accuracy rate of the fruit bruise detection system, this study used manually selected regions of interest in the fluorescence images ($Area_{ROI}$, circled area in fig. 9a) as the standard and compared these areas with the bruise area determined by the system ($Area_{sys}$), as shown in figures 9b to 9e. The accuracy rate of bruise area detection (Area rate) was calculated according to equation 5:

$$\text{Area rate}\ (\%) = 1 - \frac{\left|\text{Area}_{sys} - \text{Area}_{ROI}\right|}{\text{Area}_{ROI}} \times 100 \tag{5}$$

A further test determined the acceptable *M*-values for detection of bruise areas based on impact forces of 68.6, 88.2, and 107.8 N. As shown in figures 10 through 12, at 0.5 h after impact, the accuracy rate for the three impact forces when the *M*-value was 50 was less than 67.5%. However, when the *M*-value was 25 or 40, the accuracy

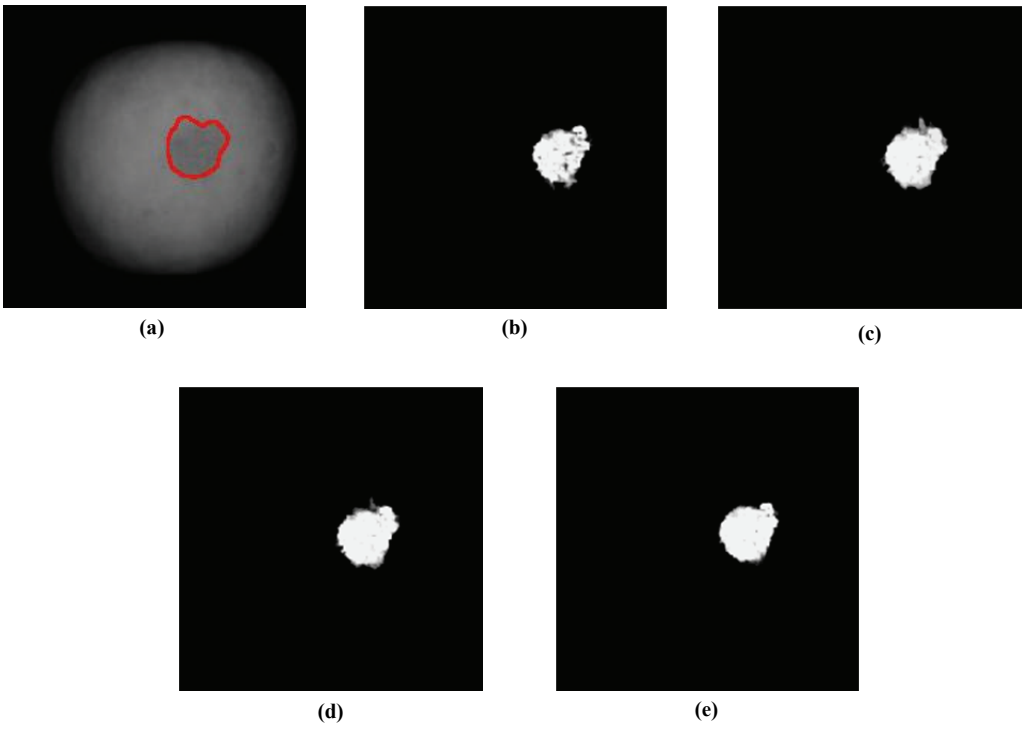

Figure 9. Detection and comparison of fruit bruise area: (a) manually selected bruise area, and bruise area determined by the automated bruise detection system at (b) 0.5 h after impact, (c) 1 h after impact, (d) 2 h after impact, and (e) 4 h after impact.

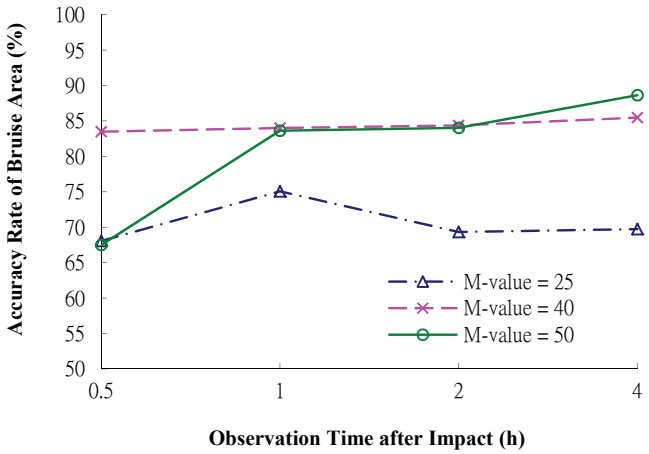

Figure 10. Effect of three *M*-values on detection accuracy of bruise area with impact force of 68.6 N.

rate was higher than 68.1%. When the *M*-value was 25, the mean accuracy rate at 2 h after impact was 75.6%, less than for the other two *M*-values (88.6% for $M = 40$ and 86.7% for $M = 50$). Considering the overall results for different observation times and impact forces, the mean accuracy rates for *M*-values of 25, 40, and 50 were 74.6%, 83.1%, and 79.3%, respectively. Finally, considering the variation in the accuracy rate of bruise area detection with time and impact force, the highest accuracy rate with the smallest variation was selected as the preferred mask size. Thus, this study used an *M*-value of 40 for detecting apple bruise areas.

Effect of Accumulated Number of Images

A fluorescence image was captured every second at 0.5 h after the apple was impacted, and the bruise features were determined by accumulating images from 5 to 60 s. The optimal accumulated image calculation was determined by comparing the accuracy rates of bruise area detection with the three impact forces. As shown in figure 13, when the number of accumulated images exceeded 20, the average accuracy rate of bruise area detection for the three impact forces exceeded 60%. When the number of accumulated images was 40, the average accuracy rate of bruise

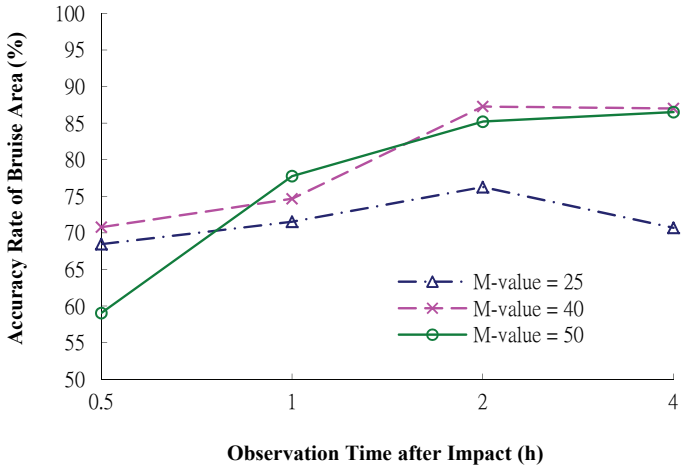

Figure 11. Effect of three *M*-values on detection accuracy of bruise area with impact force of 88.2 N.

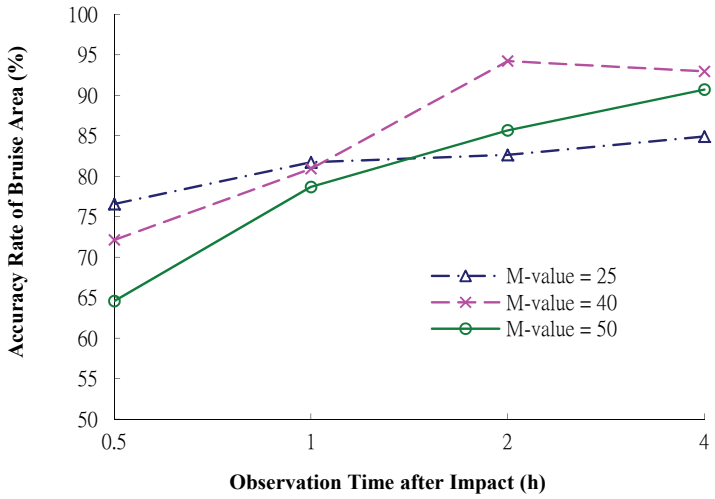

Figure 12. Effect of three *M*-values on detection accuracy of bruise area with impact force of 107.8 N.

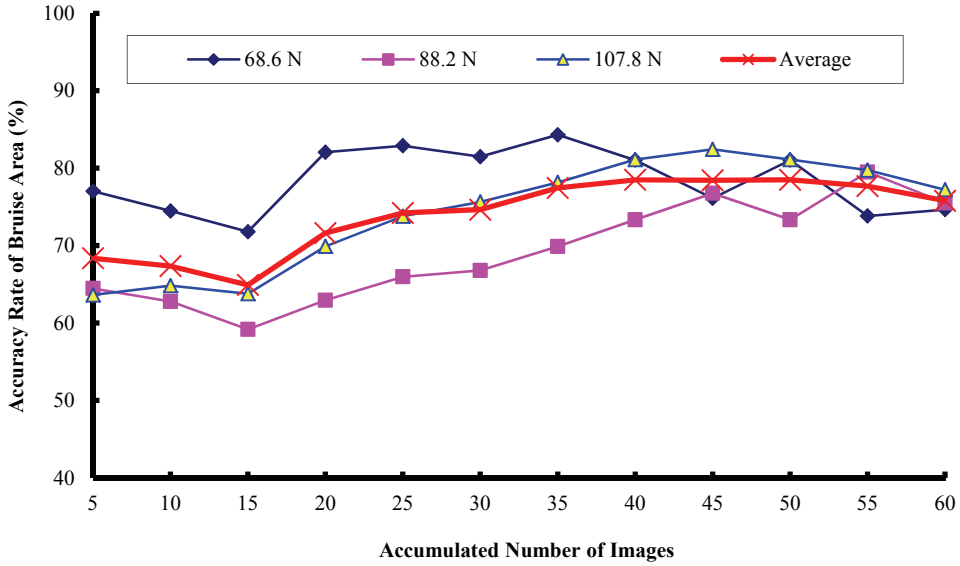

Figure 13. Detection accuracy of bruise area with accumulated number of images.

area detection for the three impact forces reached a maximum of 78.5%. The more accumulated images, the more processing time was needed, and the processing efficiency declined. The overall average accuracy rate of bruise area detection for the three impact forces was 74%. The accuracy value that was closest to the overall average accuracy of bruise area detection occurred at 25 accumulated images (accuracy rate of 74.2%). Therefore, this study used 25 accumulated mages as the basis for detecting apple bruise features.

Analysis of Overlap Rate of Bruise Area

This test used the bruise overlap rate for analysis of bruise contour edges. The manually circled region of interest in the fluorescence image (P_{ROI}) was used as the real bruise contour and was compared with the bruise contour detected (P_{sys}) by the automated system developed in this study. The bruise overlap region between the two contours was calculated to determine the overlap of the bruise area. The calculation method is shown in equation 6:

$$\text{Overlap}(\%) = \frac{P_{sys}(i,j) \cap P_{ROI}(i,j)}{P_{sys}(i,j) \cup P_{ROI}(i,j)} \times 100\% \quad (6)$$

Figures 14 through 16 show the bruise area and bruise overlap accuracy rates for the automated detection system at different observation times after impact with the three impact forces. At 0.5 h after impact, the bruise overlap accuracy for the three impact forces was between 63.1% and 75.5%, and the bruise area accuracy was greater than 70.8%. The bruise area contour is more prominent at 1 h after impact, so the bruise overlap accuracy increased to greater than 79.6%, and the bruise area accuracy was greater than 72.7%. Because bruised apple peel changes color more gradually after 1 h, the variation in the bruise area contour in the fluorescence images also became steadier. At 4 h after impact, the mean bruise overlap accuracy was greater than 87.8%, and the mean bruise area accuracy was greater than 91.2%.

Analysis of Bruise Detection Rate

The purpose of this test was to determine when chloro-

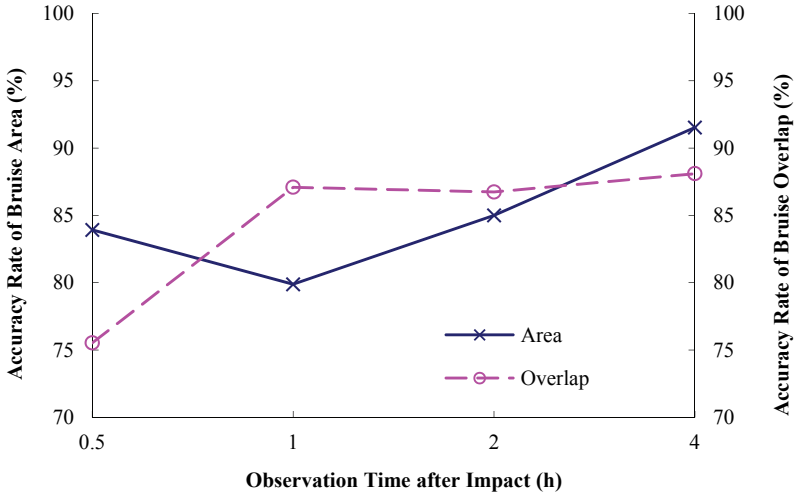

Figure 14. Detection accuracy of bruise contour area with impact force of 68.6 N.

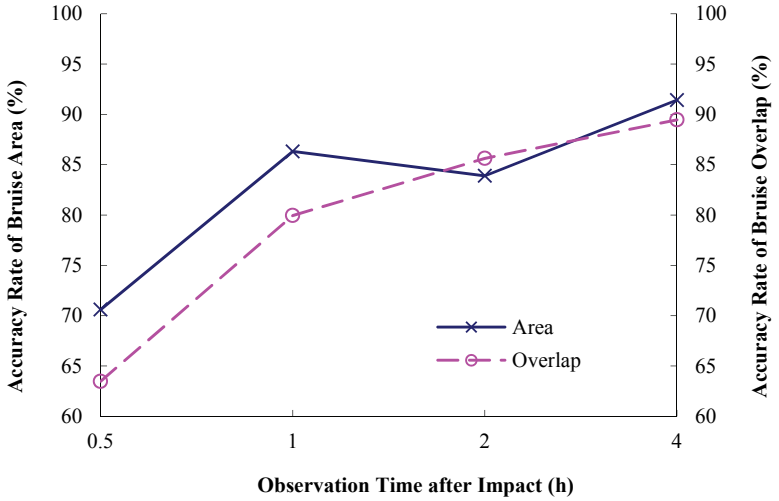

Figure 15. Detection accuracy of bruise contour area with impact force of 88.2 N.

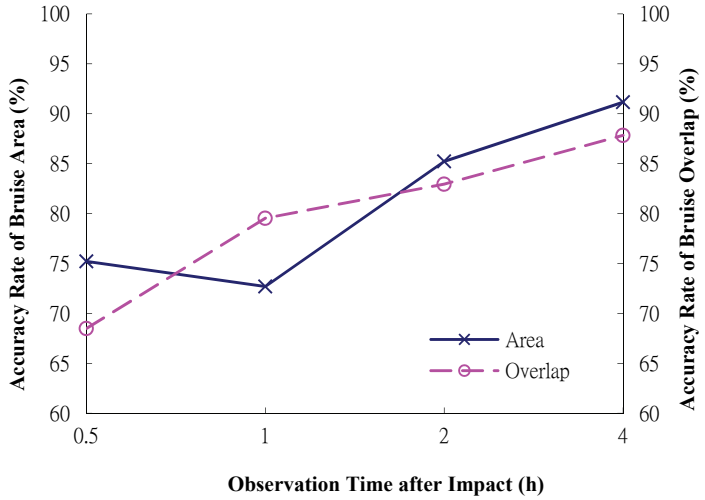

Figure 16. Detection accuracy of bruise contour area with impact force of 107.8 N.

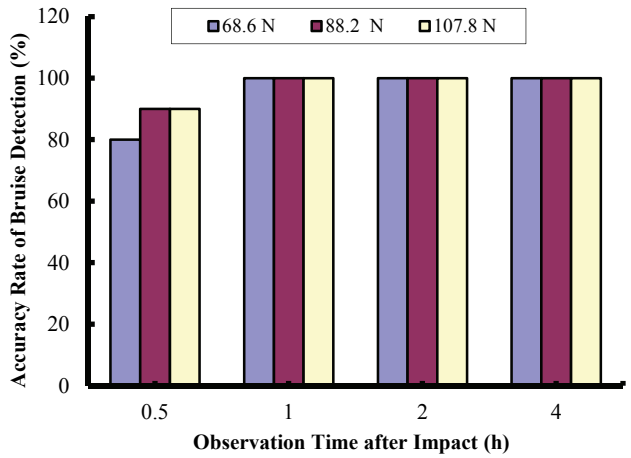

Figure 17. Detection accuracy of bruises after impacts.

phyll damage could be detected after a mechanical impact using the automated system developed in this study. The test used impact forces of 68.6, 88.2, and 107.8 N to create bruises, and each test used ten apples. A total of 25 accumulated fluorescence images were captured at 0.5, 1, 2, and 4 h after impact. The manually circled bruise area on the fluorescence image was used as the reference to determine whether the bruise area detected by the system was greater than 60% of the reference value. If so, then the proposed system could identify fruit with bruises. At 0.5 h after impact, the bruise detection rate for the 68.6 N impact force was 80%, the detection rate for the 88.2 and 107.8 N impact forces was 90%, and the mean detection rate was 86.7%. At 1 h after impact, the bruise detection rate for all three impact forces was 100% (fig. 17).

CONCLUSION

This study developed a fruit bruise detection system based on chlorophyll fluorescence images for application in quality control. Golden Delicious apples were impacted with forces of 68.6, 88.2, and 107.8 N. The bruise images were processed using local binarization and noise reduction, after which the features of the bruise area were highlighted by averaging the images.

The objective of the research was to determine the earliest point in time at which bruises could be detected with high accuracy. The results showed that the detection accuracy of bruises was 86.7% at 30 min after impact and increased to 100% at 1 h after impact. The bruise detection method developed in this study has potential to be applied to other apple varieties or other fruits. The results will also aid in the design of an on-line apple bruise detection system for real-world application in the future.

ACKNOWLEDGEMENTS

We would like to express our thanks to the National Science Council of Taiwan for funding this project. We would like to thank Professor G. J. Wu for his kind suggestions. Thanks are also extended to C. F. Lin, G. Y. Chen, and B. Y. Yang, who are students at National Ilan University, Taiwan, for their kind assistance.

REFERENCES

Ariana, D., Guyer, D. E., & Shrestha, B. (2006). Integrating multispectral reflectance and fluorescence imaging for defect detection on apples. *Computers Elec. Agric., 50*(2), 148-161. http://dx.doi.org/10.1016/j.compag.2005.10.002.

Bron, I. U., Ribeiro, R. V., Azzolini, M., Jacomin, A. P., & Machado, E. C. (2004). Chlorophyll fluorescence as a tool to evaluate the ripening of 'Golden' papaya fruit. *Postharvest Biol. Tech., 33*(2), 163-173. http://dx.doi.org/10.1016/j.postharvbio.2004.02.004.

Chen, M. T. (2009). Study of the bruise detection system for apples using fluorescence image. MS thesis. Yilan, Taiwan: National Ilan University, Department of Biomechatronic Engineering.

El Masry, G., Wang, N., Qiao, C. V., & ElSayed, A. (2008). Early detection of apple bruises on different background colors using hyperspectral imaging. *LWT - Food Sci. Tech., 41*(2), 337-345. http://dx.doi.org/10.1016/j.lwt.2007.02.022.

Jacobi, K. K., MacRaec, E. A., & Hetheringtonb, S. E. (1998). Early detection of abnormal skin ripening characteristics of 'Kensington' mango (*Mangifera indica* Linn.). *Sci. Hort., 72*(3-

4), 215-225. http://dx.doi.org/10.1016/S0304-4238(97)00135-0.
Ma, Y., Huang, M., Zhu, Q., Li, Y., & Bu, P. (2014). Recognition of bruise and pest infestation apple based on hyperspectral imaging technique. ASABE Paper No. 141908135. St. Joseph, Mich.: ASABE.
Martinsen, P., Oliver, R., Seelye, R., McGlone, V. A., Holmes, T., Davy, M., Johnston, J., Hallett, I., & Moynihan, K. (2014). Quantifying the diffuse reflectance change caused by fresh bruises on apples. *Trans. ASABE, 57*(2), 565-572. http://dx.doi.org/10.13031/trans.57.10355.
Moshou, D., Wahlen, S., Strasser, R., Schenk, A., De Baerdemaeker, J., & Ramon, H. (2005). Chlorophyll fluorescence as a tool for online quality sorting of apples. *Biosyst. Eng., 91*(2), 163-172. http://dx.doi.org/10.1016/j.biosystemseng.2005.03.008.
Nedbal, L., Soukupová, J., Whitmarsh, J., & Trtílek, M. (2000). Postharvest imaging of chlorophyll fluorescence from lemons can be used to predict fruit quality. *Photosynthetica, 38*(4), 571-579. http://dx.doi.org/10.1023/A:1012413524395.
Ostu, N. (1979). A threshold selection method from gray-level histogram. *IEEE Trans. Syst. Man Cybernetics, SMC9*(1), 62-66.
Rehkugler, G. E., & Throop, J. A. (1986). Apple sorting with machine vision. *Trans. ASAE, 29*(5), 1388-1397. http://dx.doi.org/10.13031/2013.30327.
Song, J. D., Beaudry, R. M., & Armstrong, P. R. (1997). Changes in chlorophyll fluorescence of apple fruit during maturation, ripening, and senescence. *J. Agric. Food Chem., 45*(1), 891-896.
Xing, J., & Baerdemaeker, J. D. (2007). Fresh bruise detection by predicting softening index of apple tissue using VIS/NIR spectroscopy. *Postharvest Biol. Tech., 45*(2), 176-183. http://dx.doi.org/10.1016/j.postharvbio.2007.03.002.
Xing, J., Bravo, C., Jancsók, P. T., Ramon, H., & De Baerdemaeker, J. (2005). Detecting bruises on 'Golden Delicious' apples using hyperspectral imaging with multiple wavebands. *Biosyst. Eng., 90*(1), 27-36. http://dx.doi.org/10.1016/j.biosystemseng.2004.08.002.